Archive of SID

J Nanostruct 6(3): 190-198, Summer 2016

RESEARCH PAPER

# Effect of Morphology on the Photocatalytic Behavior of ZnO Nanostructures: Low Temperature Sonochemical Synthesis of Ni Doped ZnO Nanoparticles

*Maryam Bordbar*[*,1], *Solmaz forghani-Pilerood*[2], *Ali Yeganeh-Faal*[2], *Bahar Khodadadi*[1]

[1]*Department of Chemistry, Faculty of Science, University of Qom, Qom, Iran*

[2] *Department of Chemistry, Faculty of Science, Payame Noor University, Tehran, Iran*

**ARTICLE INFO**

***Article History:***
*Received 17 April 2016*
*Accepted 28 May 2016*
*Published 1 July 2016*

***Keywords:***
*Band gap*
*Ni-ZnO nanostructure*
*Photocatalytic activity*
*Sonochemical method*

**ABSTRACT**

In the present study, ZnO nanostructure has been synthesized by different methods, namely coprecipitation, hydrothermal and sonochemical methods. After comparison of the morphology and photocatalytic activity of ZnO samples prepared via different methods, the best method (sonochemical method) was used for synthesis of Ni-ZnO nanoparticles with different concentrations of nickel. Furthermore, structural and optical properties were investigated by Fourier Transform Infrared spectroscopy, UV–Vis spectroscopy, Field Emission Scanning Electron Microscopy, X-Ray Diffraction, and Photoluminescence spectroscopy methods. Morphology of nanoparticles prepared via sonochemical method were obtained small granular shape. In addition, the direct band gap has been calculated by Tauc's approach. Compared with pure ZnO, the band gap of the Ni-ZnO NPs is smaller and depends on the content of dopants. Moreover, photocatalytic activity of all samples has been investigated under UV irradiation in an aqueous medium. In addition, photocatalytic activity is improved in the presence of an appropriate amount of nickel dopant.

**How to cite this article**
*Bordbar. M, Forghani-Pilerood. S, Yeganeh-Faal. A, Khodadadi. B. PEffect of morphology on the photocatalytic behavior of ZnO nanostructures: low temperature sonochemical synthesis of Ni doped ZnO nanoparticles. J Nanostruct, 2016; 6(3):190-198. DOI: 10.7508/JNS.2016.03.003*

## INTRODUCTION

Metal oxides such as ZnO nanostructures have attracted much attention due to their unique properties, which make them attractive candidates for wide applications in room temperature, blue and UV optoelectronic devices, ultraviolet laser emission [1], piezoelectricity [2], photocatalysis [3], solar cells [4], gas sensing [5], biological applications [6] and so on [7-10].

Dyes widely used in textiles, plastics, paper, and rubber industries, have led to water pollution due to the release of the colored and toxic wastewater into water bodies [11]. The treatment of dye waste effluents is usually inefficient, costly and non-destructive or just transfers pollution from water to another phase. Therefore, a great deal of attention has been focused on ZnO nanostructures. Properties of ZnO nanostructures are strongly dependent on the morphology of ZnO and recombination rate of the photogenerated electron–hole. Consequently, the synthetic method and metal doping are affected by these properties [12, 13].

Various methods have been developed for the synthesis of ZnO. Some of these methods such as thermal evaporation [14], chemical vapor deposition [15], and pulsed laser deposition [16] are physical ones, which generally require special and

* *Corresponding Author Email: M.Bordbare@gmail.com*

www.SID.ir

Archive of SID



expensive equipment or operation control. Others include solution based chemical methods such as coprecipitation, hydrothermal, solvothermal [17, 18], sol-gel [19-22], and sonochemical methods [20, 23], which are very attractive because of their distinct advantages such as simplicity, low cost, mild synthetic conditions and potential for large scale production [24].

Among a variety of methods, coprecipitation, hydrothermal and sonochemical methods are effective preparation methods not only for developing basic science, but also for providing a simple and effective way to control the various shapes and sizes of the ZnO powders [7, 24].

In this paper, we deal with ZnO nanostructures, which have been synthesized by different methods namely coprecipitation, hydrothermal and sonochemical methods starting from aqueous zinc acetate as the source of zinc, and reaction with an aqueous solution of NaOH as the source of oxygen without using any capping molecule. Furthermore, after comparison of the morphology and photocatalytic activity of ZnO samples prepared via different methods, the best method has been used for synthesis of Ni-ZnO (with different concentrations of nickel) and then structural and optical properties and photocatalytic activity of samples have been measured. To date, based on our knowledge there is no report on the compare of different synthesis method on photocatalytic activity of ZnO.

## MATERIALS AND METHODS

Zinc acetate dihydrate ($Zn(Ac)_2.2H_2O$), sodium hydroxide (NaOH) and nickel nitrate tetrahydrate ($Ni(NO_3)_2.4H_2O$) were obtained from Merck Chemical Company.

The sample structures were characterized by XRD patterns obtained on a Philips model X'PertPro X-ray diffractometer using Cu Kα radiation (λ=1.54 Å), while the morphologies of the synthetic samples were investigated by field emission scanning electron microscopy (FESEM; TESCAN-MIRA3) equipped with an Oxford Inca Energy Dispersive X-ray detector. The optical absorptions of the samples were obtained using a Shimadzu UV-2500 spectrophotometer. Fourier transform infrared spectra (FTIR) of the samples were recorded using a Jasco model 4200 FTIR spectrophotometer over the frequency range of 400-4000 $cm^{-1}$ using KBr as the diluent. The room temperature photoluminescence (RT-PL) measurements were performed on a Cary Eclipse fluorescence spectrophotometer with a wavelength of 325 nm as the excitation source. In order to evaluate the photocatalytic activity of the samples, methyl orange (MO) degradation was evaluated as follows: Before the illumination, a 5 ppm solution of MO was magnetically stirred in the dark for 1 h to ensure the establishment of absorption equilibrium of methyl orange on the photocatalyst sample surfaces. Following this, the suspension was irradiated under a 50 W low pressure Hg lamp. UV-Vis absorption spectra were recorded at different times to calculate MO concentrations

*Sample preparation*

ZnO nanostructure synthesis by coprecipitation method. The typical procedure for the preparation of samples using coprecipitation method was as follows:

First, 25 mL of a 0.1 M aqueous solution of zinc acetate in a beaker were stirred magnetically at room temperature on an ice bath. The white precipitate was filtered, thoroughly washed with distilled water, dried in an oven at 60 °C for 1 h and ultimately calcined at 300 °C for 1 h.

*ZnO nanostructure synthesis hydrothermal method*

First, 25 mL of a 0.1 M aqueous solution of zinc acetate in a beaker were stirred magnetically at room temperature on an ice bath. Then, 100 mL of a 0.1 M aqueous solution of sodium hydroxide was added to this solution dropwise for about 45-50 min. Finally, the white precipitate formed was transferred to an autoclave and maintained at 95 °C for 20 h and then allowed to cool to room temperature. The white precipitate was filtered, thoroughly washed with distilled water and dried in an oven at 60 °C for 1 h.

*ZnO NPs synthesis by sonochemical method*

Samples were synthesized by a simple sonochemical method using a sonochemical bath. The procedure was as follows: First, 25 mL of a 0.1 M aqueous solution of zinc acetate in a beaker on an ice bath, was kept in a sonication bath (28 kHz, 340 W). Then, 100 mL of a 0.1 M aqueous solution of sodium hydroxide was added to this solution dropwise for about 45-50 min. Finally, the white precipitate was filtered, thoroughly washed with distilled water and dried in an oven at 60 °C for 1 h. In the presence of ultrasound following reaction take place:

$Zn^{2+} + 4OH^- \longleftrightarrow [Zn(OH)_4]^{2-}$



www.SID.ir

Archive of SID



$$2\,[Zn(OH)_4]^{2-} \xrightarrow{)))} 2ZnO + 4H_2 + 3O_2$$

*Ni-ZnO NPs synthesis by sonochemical method*

All the steps in the synthesis of Ni-ZnO NPs were similar to those for ZnO NPs, but appropriate amounts of Ni acetate ([Ni]/[Zn]%=0.25, 0.5 and 0.75%) were added to aqueous zinc acetate solution in the first step.

## RESULTS AND DISCUSSION

*Sample characterization*

FE-SEM images were used to describe the morphologies. Fig. 1 shows the FE-SEM images of ZnO nanostructure prepared using different methods.

FE-SEM images reveal that the ZnO samples prepared using coprecipitation and hydrothermal methods consist of aggregates of particles with irregular sizes and shaped agglomerated particles in the nano/micro-scale range, whereas typical FE-SEM images of ZnO sample prepared via sonochemical method indicate that particles are very uniform and have spherical shapes with the diameters varying between 65 to 70 nm [25, 26] (see particle size distribution, inset Fig. 1).

The sonochemical method has been proved to be a useful method to obtain novel materials. The chemical effects of ultrasonic irradiation arise from acoustic cavitation, in other words, the formation,

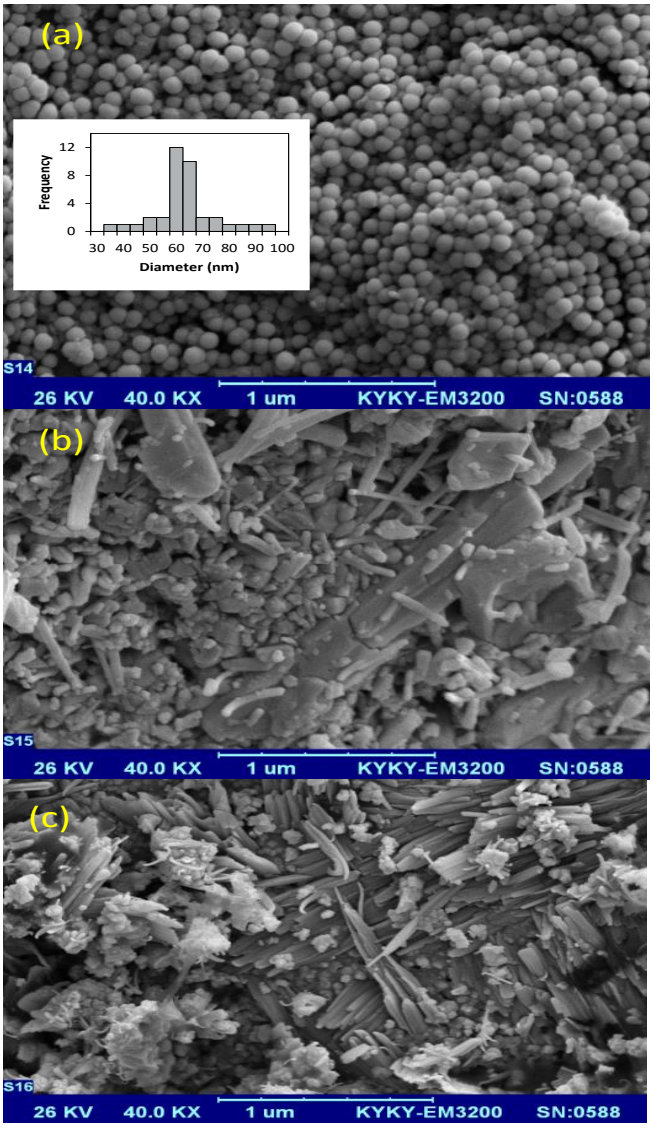


Fig. 1. FE-SEM images of ZnO samples prepared by different methods: (a) sonochemical (b) hydrothermal (c) coprecipitation.



www.SID.ir

Archive of SID



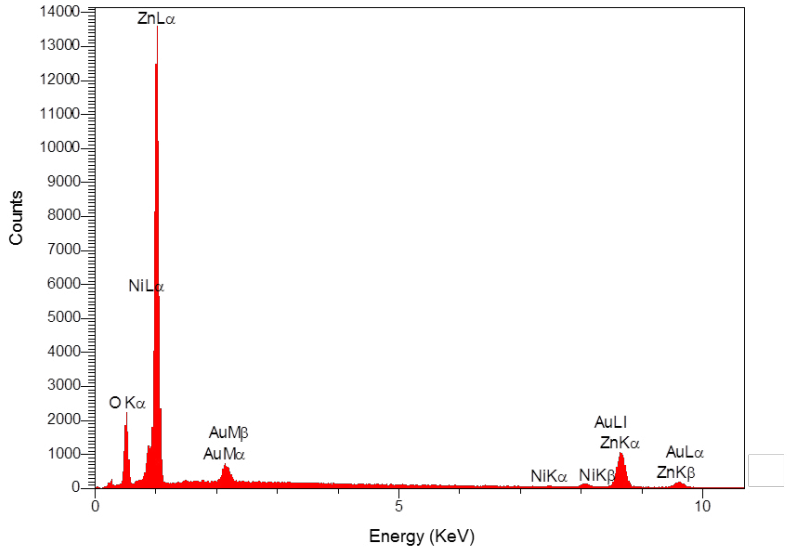


Fig. 2. Typical EDAX pattern obtained for the Ni-ZnO (0.50%) NPs.

growth and implosive collapse of bubbles in a liquid medium, which results in an instantaneously high temperature and pressure pulse. These special conditions of high temperature, pressure and local intense micromixing attained during acoustic cavitation lead to many unique properties in the irradiated solution and particles suspended in the same [27].

The composition of ZnO and Ni-ZnO NPs were determined by the elemental dispersion analysis using X-ray (EDX) measurements. The EDX results for Ni-ZnO samples confirm the presence and uniform distribution of the elements zinc, nickel and oxygen (Fig. 2).

The characteristic functional groups of ZnO samples prepared using different methods and Ni-ZnO NPs (with different concentrations of Ni) prepared via sonochemical method were investigated using FTIR spectroscopy at room temperature in the range of 4000-400 $cm^{-1}$ and the results are shown in Fig. 3.

The broad peak observed in the 460–560 $cm^{-1}$ range is the combination of Zn-O vibrations. The vibration mode at 475 $cm^{-1}$ has changed slightly in Ni-ZnO samples. It seems the change is related to the interaction between ZnO and metal ions, which has formed new bonds. Moreover, in Ni-ZnO samples, no obvious changes can be seen in FTIR spectra of undoped and doped samples. It is worth mentioning that Ni atoms were successfully incorporated into the crystal lattice of ZnO. Therefore, it is reasonable to conclude that synthetic product has no significant impurity [28].

The X-ray diffraction patterns of samples are shown in Fig. 4. The diffraction patterns of samples prepared via different methods well match with hexagonal wurtzite structure [29, 30].

Comparison of the spectrum of pure ZnO with that of Ni-ZnO indicates that the samples are single phase with a hexagonal wurtzite without formation of impurities like NiO. It seems that the doping with $Ni^{2+}$ ions has no appreciable effect on the crystal phase of ZnO [31].

The diffraction peaks of Ni-ZnO samples are shifted slightly to higher angles with increasing Ni concentration. The small shift of peaks to higher values is reasonable because the ionic radius of $Ni^{2+}$ ion (0.055 nm) is only slightly less than that of $Zn^{2+}$ ion (0.060 nm) at tetrahedral site. Therefore, the substitution of $Ni^{2+}$ ion for $Zn^{2+}$ will not result in much distortion in the ZnO lattice, generally [32].

The lattice parameters of samples are found using the following equation [32].

$$\frac{1}{d^2} = \frac{4}{3}\left(\frac{h^2 + hk + k^2}{a^2}\right) + \frac{l^2}{c^2} \qquad (1)$$

Where h, k and l are Miller indexes and d is the distance between adjacent lattice planes in the crystal.

Table 1 shows the calculated lattice parameters of the samples. Lattice parameters of Ni-ZnO are slightly less than those of ZnO, confirming that the Ni ions have been doped into the ZnO crystal lattice without changing the wurtzite structure. On



www.SID.ir

Archive of SID



the other hand, zinc and nickel have ionic radii of 0.60 and 0.55 Å, respectively. Hence, if Ni replaces Zn in the ZnO crystal lattice, a little reduction in lattice parameters is expected [33].

In addition, according to the Scherrer formula ($D = k\lambda/\beta\cos\theta$) [34], the average crystallite size of ZnO NPs prepared using sonochemical method associated with the all diffraction peaks was estimated about 19.2 nm.

*Optical properties of samples*

To confirm the optical properties of the ZnO nanostructures prepared using different methods and Ni-ZnO nanostructure (with different concentrations of Ni) prepared via sonochemical method, the UV-Vis transmittance spectra were also recorded and the results are presented in Fig. 5. [35]. It can be clearly seen that in all samples, the sharp absorption edge at the wavelength of about 370 nm can be assigned to the intrinsic band gap absorption for the wurtzite hexagonal structure of ZnO. In addition, according to Fig. 5(b), comparison of the UV-Vis spectra of undoped ZnO and Ni doped with different concentrations of dopant, the maximum of the absorbance band show slight red shifts due to nickel doping and increasing Ni content causes a slight blue shift in band edge absorption peak. The wavelengths of maximum absorbance for each nanostructure sample are listed in Table 1.

The absorption coefficients of samples were investigated by Tauc's approach and the optical band gap of the ZnO nanostructures prepared using different methods and Ni-ZnO nanostructure (with different concentrations of Ni) prepared via sonochemical method were calculated using the following equation [19]:

$(\alpha h\nu)^2 = C(h\nu - E_g)$

where α is the absorption coefficient, C is a constant, hν is the photon energy and $E_g$ is the band gap. Fig. 6 shows the Tauc plots of samples. Extrapolation of the linear region of Tauc plot gives a band gap. The absorption spectra are

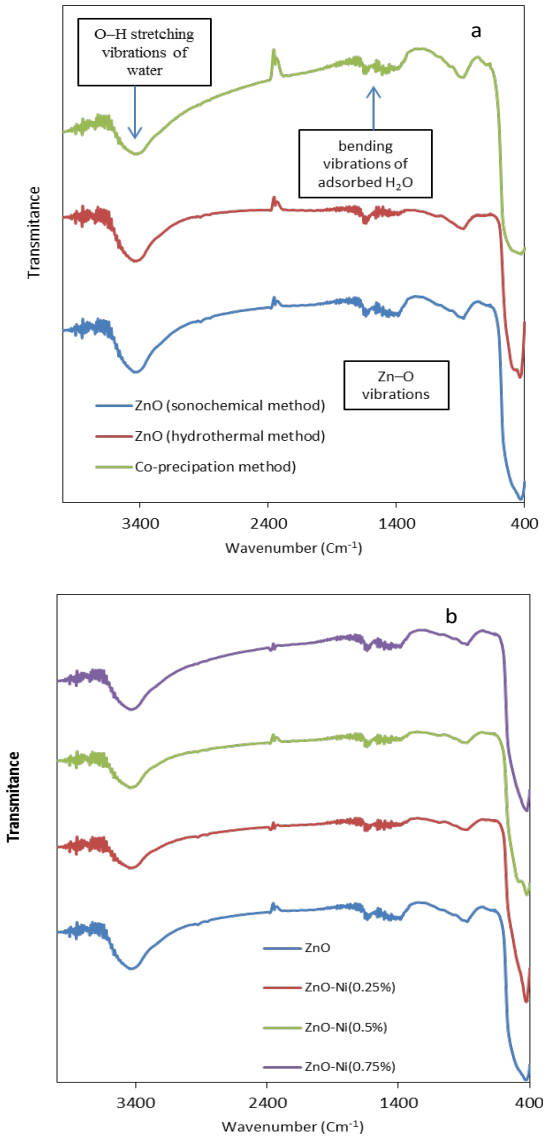


Fig. 3. FTIR spectra of samples: (a) ZnO samples (different methods), (b) Ni-ZnO NPs (sonochemical method).

shown in Fig. 6. When the concentration of Ni-doping increases, the band gap first decreases and then increases (Table 1), while the doping level

Table 1. Peak position, band gap, lattice constants and photcatalytic activity of samples.

| Samples | EDAX analysis % | a (100) | c (002) | Wavelength (nm) | Bandgap (eV) | Degradation in 180 min |
|---|---|---|---|---|---|---|
| ZnO (precipitation) | 0.00 | 3.2359 | 5.1872 | 374 | 2.47 | 58% |
| ZnO (hydrothermal) | 0.00 | 2.2478 | 5.2055 | 370 | 3.08 | 60% |
| ZnO (sonochemical) | 0.00 | 3.2416 | 5.1962 | 372 | 2.97 | 78% |
| ZnO-Ni (0.25%) | 0.21 | 3.2378 | 5.1918 | 374 | 2.95 | 92% |
| ZnO-Ni (0.50%) | 0.49 | 3.2410 | 5.1957 | 376 | 2.92 | 100% |
| ZnO-Ni (0.75%) | 0.69 | 3.2387 | 5.1899 | 370 | 3.00 | 62% |



www.SID.ir

Archive of SID



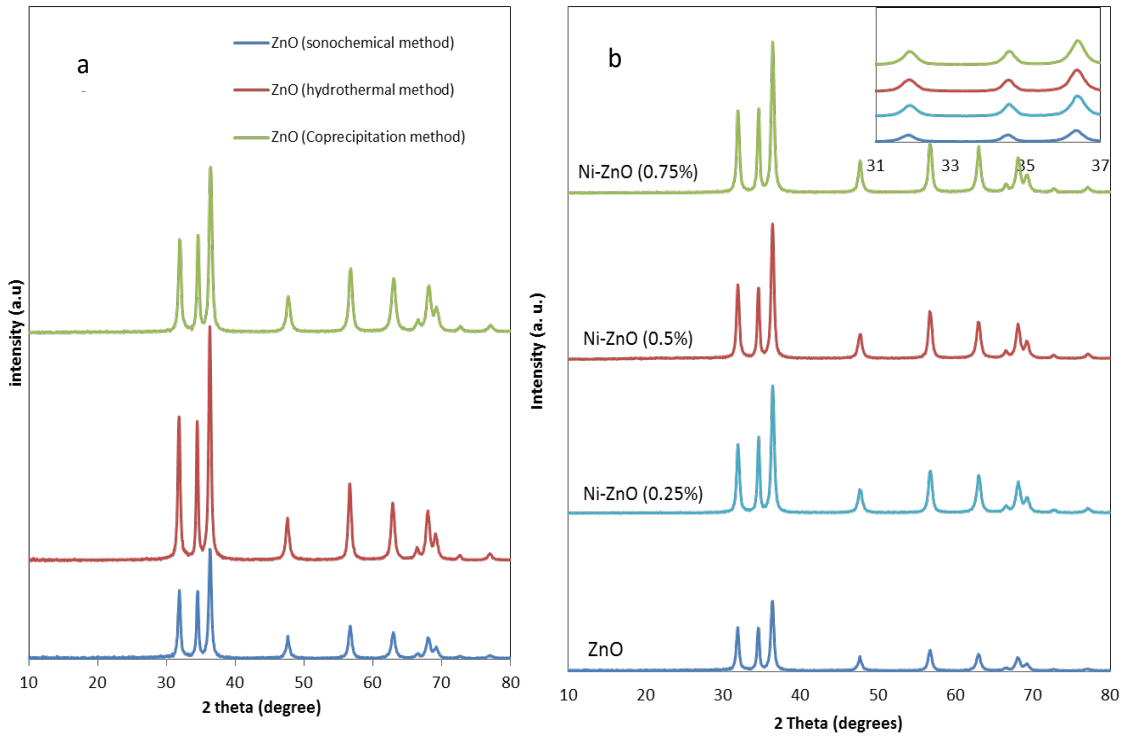


Fig. 4. XRD spectra of samples: (a) ZnO samples (different methods), (b) Ni-ZnO NPs (sonochemical method).

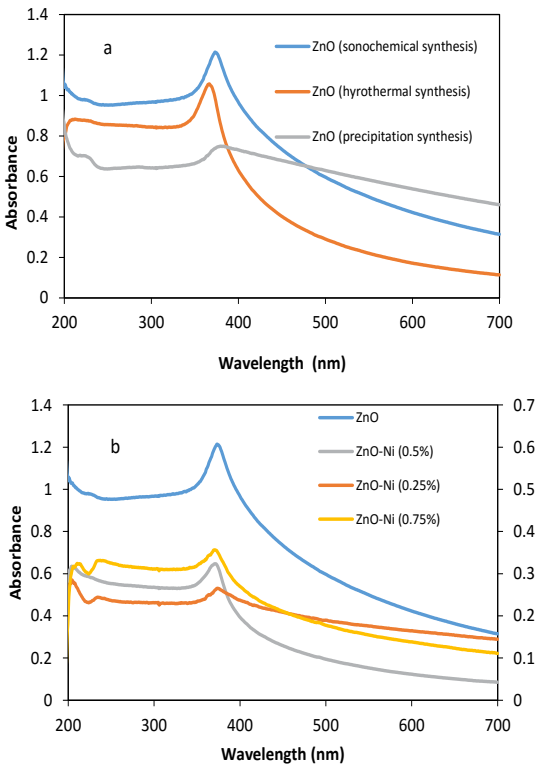


Fig. 5. UV-Vis spectra of samples: (a) ZnO samples (different methods), (b) Ni-ZnO NPs (sonochemical method).

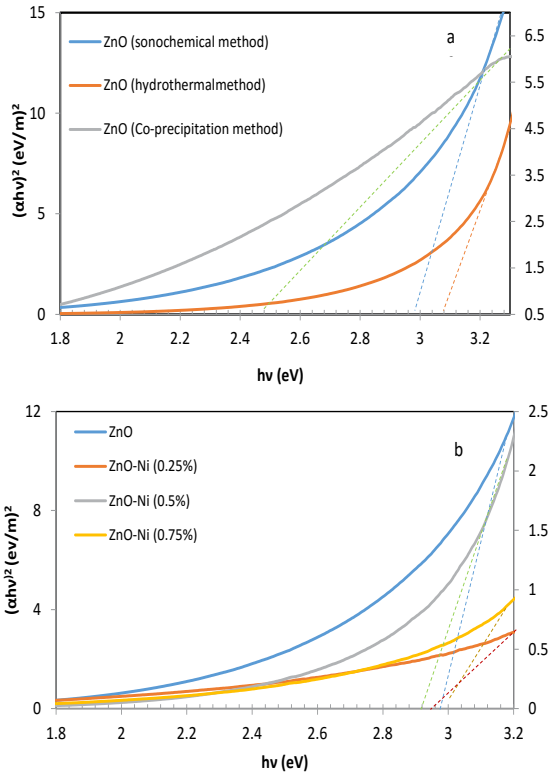


Fig. 6. The Tauc plots of samples: (a) ZnO samples (different methods), (b) Ni-ZnO NPs (sonochemical method).



www.SID.ir

Archive of SID



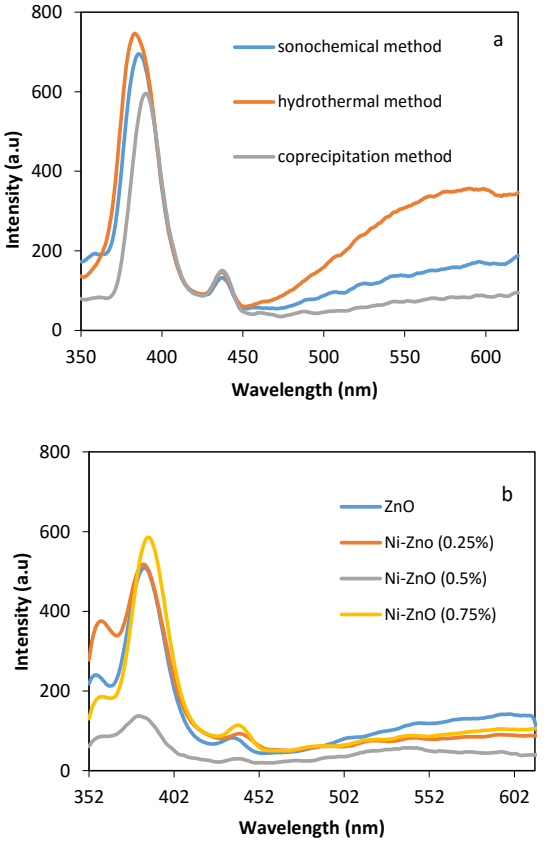


Fig. 7. The PL spectra of samples: (a) ZnO samples (different methods), (b) Ni-ZnO NPs (sonochemical method).

is (> 0.5%), which is because the excess carriers provided by dopingcan fill some energy levels on the edge of conduction band and cause the transition energy increase [32]. Furthermore, sp–d exchange interactions are responsible for the band gap variations in Ni- ZnO samples.

Room temperature PL spectra of the samples are shown in Fig. 7. As shown in Fig. 7, all samples have two peaks at about 380 nm (near-band edge emission (NBE), which come from the collision of the free excited electrons and holes) and 570 nm (deep level emission (DLE) mediated by oxygen vacancies and other defects). Since PL emission is the result of the recombination of excited electrons and holes, the lower PL intensity of the sample indicates a lower recombination rate of excited electrons and holes [36-38].

PL spectra of the samples prepared by different methods (Fig. 7(a)) show that the intensity of the deep level emission (DLE) band for the sample prepared by hydrothermal method is higher than that of other samples. It can be deduced that oxygen vacancies and other defects in this sample are higher than those in other samples. Moreover, Fig. 7(b) shows that in Ni-ZnO (0.5%) sample, the near-band edge emission (NBE) peak intensity decreases, probably due to less recombination rate.

*Photocatalytic activity*

In order to evaluate the photocatalytic activity of the samples, photodegradation of methyl orange (MO) under UV light irradiation was performed in the presence of samples at room temperature and the results are shown in Fig. 8.

As observed in Fig. 8(a), ZnO nanostructure prepared by the sonochemical method showed better photocatalytic activity than that by the coprecipitation or hydrothermal methods.

As we know, particle size and surface area have key effects on the photocatalytic activities of photocatalyst. Expect these factors, which play important roles in photocatalytic activity, however, other parameters such as morphology, defect and impurity contents might affect photocatalytic activity [39].

On the basis of the FE-SEM results, specific surface areas of the samples prepared by

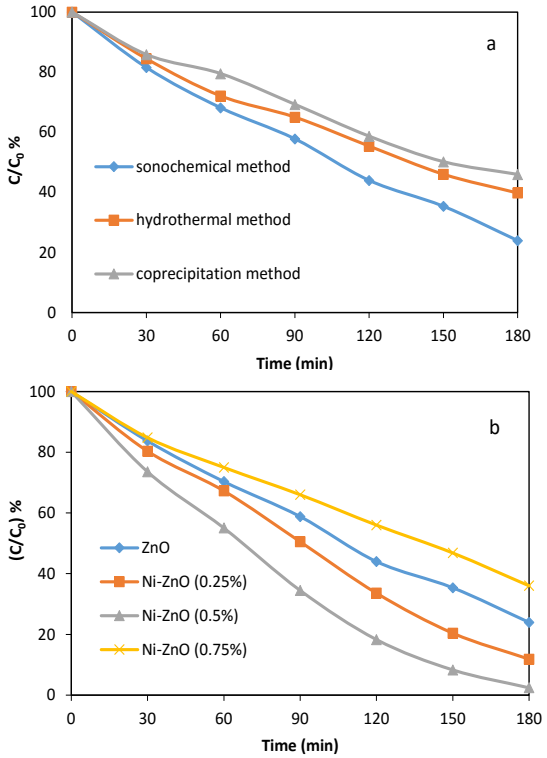


Fig. 8. Photodegradation of methyl orange (MO) using the samples: (a) ZnO samples (different methods), (b) Ni-ZnO NPs (sonochemical method).





www.SID.ir

Archive of SID



sonochemical method are larger than those of other samples indicating the better photocatalytic activity of this sample.

According to Fig. 8(b), the degradation rate increases depending on the Ni content, and a 0.5% content of Ni resulted in the highest photodegradation of the MO dye. This efficiently reduces the recombination chance of excitions so that the doping induces the distortion of local electric field and the photo induced electrons and holes could be trapped around the dopant, which is in good agreement with the PL results [32].

## CONCLUSION

Zinc oxide nanopowder has been synthesized by different methods and used as a catalyst in the process of photodegradation of methyl orange as a dye model. According to the results, samples prepared via sonochemical method in low temperature and short time (2 h) have an average diameter of 60- 70 nm and are very uniform, have spherical shapes and show the best photocatalytic activity in comparison with those prepared by hydrothermal or coprecipitation methods. Sonochemical method does not require pressure controlling and high temperature. Moreover, Ni-doped ZnO (with different concentrations of nickel) has been synthesized by sonochemical method. Results indicate that the presence of a small amount of nickel in ZnO structure enhances the photodegradation efficiency, but further increase of the dopant concentration results in a decrease in photocatalytic activity.

## ACKNOWLEDGEMENTS

The author is thankful to Iran National Science Foundation (INSF) for supporting this project numbered 90005627.

## CONFLICT OF INTEREST

The authors declare that there is no conflict of interests regarding the publication of this manuscript.

## REFERENCES

1. Versteegh MAM, Vanmaekelbergh D, Dijkhuis JI. Room-Temperature Laser Emission of ZnO Nanowires Explained by Many-Body Theory. Phys. Rev. Lett. 2012; 108(15): 157402.
2. Riaz M, Song J, Nur O, Wang ZL, Willander M. Study of the Piezoelectric Power Generation of ZnO Nanowire Arrays Grown by Different Methods. Adv. Funct. Mater. 2011; 21(4): 628-633.
3. Khataee A, Saadi S, Safarpour M, Joo SW. Sonocatalytic performance of Er-doped ZnO for degradation of a textile dye. Ultrason. Sonochem. 2015; 27: 379-388.
4. Vanalakar SA, Mali SS, Pawar RC, Dalavi DS, Mohalkar AV, Deshamukh HP, et al. Farming of ZnO nanorod-arrays via aqueous chemical route for photoelectrochemical solar cell application. Ceram. Int. 2012; 38(8): 6461-6467.
5. Liang S, Zhu L, Gai G, Yao Y, Huang J, Ji X, et al. Synthesis of morphology-controlled ZnO microstructures via a microwave-assisted hydrothermal method and their gas-sensing property. Ultrason. Sonochem. 2014; 21(4): 1335-1342.
6. Sharifalhoseini Z, Entezari MH, Jalal R. Direct and indirect sonication affect differently the microstructure and the morphology of ZnO nanoparticles: Optical behavior and its antibacterial activity. Ultrason. Sonochem. 2015; 27: 466-473.
7. Zhou K, Zhang Q, Shi Y, Jiang S, Hu Y, Gui Z. A facile method for preparation ZnO with different morphology and their optical property. J. Alloys Compd. 2013; 577: 389-394.
8. de Andrade Gomes M, Giroldo Valerio ME, Queiruga Rey JF, Macedo ZS. Comparative study of structural and optical properties of ZnO nanostructures prepared by three different aqueous solution methods. Mater. Chem. Phys. 2013; 142(1): 325-332.
9. Zhong Jb, Xu B, Feng FM, He Xy, Li Jz, Hu W. Fabrication and photocatalytic activity of ZnO prepared by different precipitants using paralled flaw precipitation method. Mater. Lett. 2011; 65(12): 1995-1997.
10. Singh S, Chakrabarti P. Comparison of the structural and optical properties of ZnO thin films deposited by three different methods for optoelectronic applications. Superlattices Microst. 2013; 64(0): 283-293.
11. Karunakaran C, Dhanalakshmi R. Phenol degradation on Pr6O11 surface under UV-A light. Synergistic photocatalysis by semiconductors. Radiat. Phys. Chem. 2009; 78(1): 8-12.
12. Evgenidou E, Konstantinou I, Fytianos K, Poulios I, Albanis T. Photocatalytic oxidation of methyl parathion over $TiO_2$ and ZnO suspensions. Catal. Today 2007; 124(3–4): 156-162.
13. Xie J, Wang H, Duan M, Zhang L. Synthesis and photocatalysis properties of ZnO structures with different morphologies via hydrothermal method. Appl. Surf. Sci. 2011; 257(15): 6358-6363.
14. Kong X, Sun X, Li X, Li Y. Catalytic growth of ZnO nanotubes. Mater. Chem. Phys. 2003; 82(3): 997-1001.
15. Tominaga K, Takao T, Fukushima A, Moriga T, Nakabayashi I. Amorphous ZnO–In2O3 transparent conductive films by simultaneous sputtering method of ZnO and In2O3 targets. Vacuum 2002; 66(3–4): 505-509.
16. Naghavi N, Marcel C, Dupont L, Rougier A, Leriche J-B, Guery C. Structural and physical characterisation of transparent conducting pulsed laser deposited InO-ZnO thin films. J. Mater. Chem. 2000; 10(10): 2315-2319.
17. Zhai H-J, Wu W-H, Lu F, Wang H-S, Wang C. Effects of ammonia and cetyltrimethylammonium bromide (CTAB) on morphologies of ZnO nano- and micromaterials under solvothermal process. Mater. Chem. Phys. 2008; 112(3): 1024-1028.
18. Bordbar M, Vasegh SM, Jafari S, Yeganeh-Faal A. Optical and photocatalytic properties undoped and Mn-doped ZnO nanoparticles synthesized by hydrothermal method: Effect of annealing temperature. Iranian Journal Of Catalysis 2015; 5(2): 135-141.
19. Bordbar M, Khodadadi B, Mollatayefe N, Yeganeh-Faal A. Journal of Applied Chemistry Influence of metal (Ag, Cd, Cu)-doping on the optical properties of ZnO nanopowder: Variation of band gap. J. Appl. Chem. 2013; 8(27): 43-48.
20. Khodadadi B, Bordbar M. Sonochemical synthesis



www.SID.ir

Archive of SID



of undoped and Co-doped ZnO nanostructures and investigation of optical and photocatalytic properties. Iran. J. Catal. 2016; 6(1): 37-42.
21. Khodadadi B, Bordbar M, sajedi M. Preparation, Characterization and Photocatalytic Activity of Ag-Cd-ZnO and Ag-Cu-ZnO Nanostructures. Journal of Applied Chemical Research 2014; 8(4): 35-44.
22. Khodadadi B, Bordbar M, Yeganeh-Faal A. Optical, structural, and photocatalytic properties of Cd-doped ZnO powders prepared via sol–gel method. J. Sol-Gel Sci. Technol. 2015; 77: 521-527.
23. Kumar RV, Diamant Y, Gedanken A. Sonochemical Synthesis and Characterization of Nanometer-Size Transition Metal Oxides from Metal Acetates. Chem. Mater. 2000; 12(8): 2301-2305.
24. Rezapour M, Talebian N. Comparison of structural, optical properties and photocatalytic activity of ZnO with different morphologies: Effect of synthesis methods and reaction media. Mater. Chem. Phys. 2011; 129(1–2): 249-255.
25. Zhu H-Y, Xiao L, Jiang R, Zeng G-M, Liu L. Efficient decolorization of azo dye solution by visible light-induced photocatalytic process using SnO2/ZnO heterojunction immobilized in chitosan matrix. Chem. Eng. J. 2011; 172(2–3): 746-753.
26. Aslani A, Arefi MR, Babapoor A, Amiri A, Beyki-Shuraki K. Solvothermal synthesis, characterization and optical properties of ZnO, ZnO–MgO and ZnO–NiO, mixed oxide nanoparticles. Appl. Surf. Sci. 2011; 257(11): 4885-4889.
27. Pinjari DV, Pandit AB. Room temperature synthesis of crystalline CeO2 nanopowder: Advantage of sonochemical method over conventional method. Ultrason. Sonochem. 2011; 18(5): 1118-1123.
28. Ghosh CK, Malkhandi S, Mitra MK, Chattopadhyay KK. Effect of Ni doping on the dielectric constant of ZnO and its frequency dependent exchange interaction. J. Phys. D: Appl. Phys. 2008; 41(24): 245113-245113.
29. Zhou X, Li Y, Peng T, Xie W, Zhao X. Synthesis, characterization and its visible-light-induced photocatalytic property of carbon doped ZnO. Mater. Lett. 2009; 63(20): 1747-1749.
30. Saravanan R, Karthikeyan S, Gupta VK, Sekaran G, Narayanan V, Stephen A. Enhanced photocatalytic activity of ZnO/CuO nanocomposite for the degradation of textile dye on visible light illumination. Mater. Sci. Eng. C 2013; 33(1): 91-98.
31. Kaneva NV, Dimitrov DT, Dushkin CD. Effect of nickel doping on the photocatalytic activity of ZnO thin films under UV and visible light. Appl. Surf. Sci. 2011; 257(18): 8113-8120.
32. Zhao J, Wang L, Yan X, Yang Y, Lei Y, Zhou J, et al. Structure and photocatalytic activity of Ni-doped ZnO nanorods. Mater. Res. Bull. 2011; 46(8): 1207-1210.
33. He R, Hocking RK, Tsuzuki T. Co-doped ZnO nanopowders: Location of cobalt and reduction in photocatalytic activity. Mater. Chem. Phys. 2012; 132(2–3): 1035-1040.
34. Bordbar M, Alimohammadi T, Khoshnevisan B, Khodadadi B, Yeganeh-Faal A. Preparation of MWCNT/TiO2–Co nanocomposite electrode by electrophoretic deposition and electrochemical study of hydrogen storage. Int. J. Hydrogen Energy 2015; 40(31): 9613-9620.
35. Liu C, Liu Z, Li Y, Liu Z, Wang Y, E L, et al. Enhanced visible-light-responsive photocatalytic property of CdS and PbS sensitized ZnO nanocomposite photocatalysts. Mater. Sci. Eng. B 2012; 177(8): 570-574.
36. Li Q, Kang Z, Mao B, Wang E, Wang C, Tian C, et al. One-step polyoxometalate-assisted solvothermal synthesis of ZnO microspheres and their photoluminescence properties. Mater. Lett. 2008; 62(16): 2531-2534.
37. Long T, Takabatake K, Yin S, Sato T. Mild solvothermal synthesis and characterization of ZnO crystals with various morphologies on borosilicate glass substrate. J. Cryst. Growth 2009; 311(3): 576-579.
38. Majeed J, Jayakumar OD, Mandal BP, Salunke HG, Naik R, Tyagi AK. Facile synthesis of flower like FePt/ZnO core–shell structure and its bifunctional properties. J. Alloys Compd. 2014; 597: 95-100.
39. Suwanboon S, Amornpitoksuk P, Sukolrat A, Muensit N. Optical and photocatalytic properties of La-doped ZnO nanoparticles prepared via precipitation and mechanical milling method. Ceram. Int. 2013; 39(3): 2811-2819.



www.SID.ir